

Domain Adaptation via CycleGAN for Retina Segmentation in Optical Coherence Tomography

Ricky Chen*
Simon Fraser University
shuo_chen_4@sfu.ca

Gavin Xu*
Simon Fraser University
jiacheng_xu_2@sfu.ca

Marinko V. Sarunic
Simon Fraser University
msarunic@sfu.ca

Timothy T. Yu*
Simon Fraser University
timothy_yu@sfu.ca

Da Ma
Simon Fraser University
da_ma@sfu.ca

Mirza Faisal Beg
Simon Fraser University
faisal_beg@sfu.ca

July 7, 2021

Abstract

With the FDA approval of Artificial Intelligence (AI) for point-of-care clinical diagnoses [1][2], the generalizability of a network’s performance is of the utmost importance as clinical decision-making must be domain-agnostic [3]. A method of tackling the problem is to increase the dataset to include images from a multitude of domains; while this technique is ideal, the security requirements of medical data is a major limitation. Additionally, researchers with developed tools benefit from the addition of open-sourced data, but are limited by the difference in domains. Herewith, we investigated the implementation of a Cycle-Consistent Generative Adversarial Networks (CycleGAN) for the domain adaptation of Optical Coherence Tomography (OCT) volumes. This study was done in collaboration with the Biomedical Optics Research Group and Functional & Anatomical Imaging & Shape Analysis Lab at Simon Fraser University. In this study, we investigated a learning-based approach of adapting the domain of a publicly available dataset, UK Biobank dataset (UKB) [1]. To evaluate the performance of domain adaptation, we utilized pre-existing retinal layer segmentation tools developed on a different set of RETOUCH OCT data. This study provides insight on state-of-the-art tools for domain adaptation compared to traditional processing techniques as well as a pipeline for adapting publicly available retinal data to the domains previously used by our collaborators.

*Equal contribution.

1 Introduction

Artificial Intelligence (AI) has caused a shift in focus towards the role of data in decision-making, and is projected to have an impact in the healthcare system. While AI has been shown to improve accuracy, specificity, and sensitivity of clinician diagnoses [4], there are many valid concerns and limitations of these systems. Alongside patient security [5], quality of care [5], and equality [5], the generalizability of these tools may be lacking [3]. As data ranges across different operators, acquisition systems, and patients, the domain-dependent performance of the deep learning tools vary and must be validated in the environment that it is used [3]. In this study, we investigate the use of a Cycle-Consistent Generative Adversarial Networks (CycleGAN) to adapt data from an external domain to the domain that our learning-based tools have been trained on. The performance of domain adaptation from UK Biobank dataset (UKB) to RETOUCH was evaluated through retina segmentation from the inner limiting membrane (ILM) to the retinal pigment epithelium (RPE).

1.1 Data Acquisition

Two datasets were used for domain adaptation. The RETOUCH dataset, which was originally published in a half day challenge, contains retinal Optical Coherence Tomography (OCT) volumes along with labels of the retinal layers, Intraretinal Fluid (IRF), Subretinal Fluid (SRF), and Pigment Epithelium Detachments (PED) [6]. The volumes were imaged using a Topcon machine, and each volume consists of 128 B-scans of size 650x512. This study utilized 13 volumes in total, which is equivalent to 1664 B-scans. UK Biobank dataset was released by UKB, which contains in-depth genetic and health information from half a million UK participants [7]. More than 80000 volumes were available in the UKB dataset, but only 13 volumes without pathological cases were chosen to be consistent with the RETOUCH dataset. Figure 1 shows sample B-scans from the two domains.

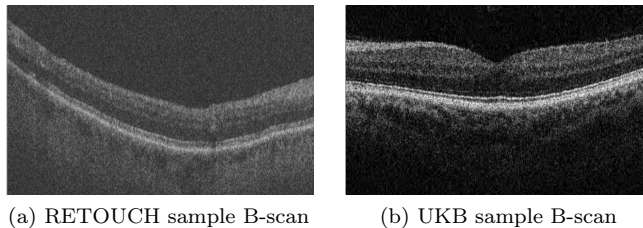


Figure 1: Comparison of two datasets/domains

As shown in the above figure, UKB appears to have undergone some denoising processes, which may include but is not limited to: 2D retina flattening, pepper noise reduction, etc.

1.2 Layer Segmentation Network

The LF-UNet, a deep neural network based on U-Net and fully convolutional network, was used as a pre-trained layer segmentation network [8]. The architecture of the U-Net leverages a symmetrical convolutional network. It consists of multiple 3x3 convolutional layers followed by a Rectified Linear Unit (ReLU) and 2x2 max pooling layer [9]. The up-sampled output is then concatenated with the corresponding cropped feature maps. The network can thus learn multiple in-depth features and perform concrete pixel-wise segmentation. In addition to a simple U-Net, LF-UNet cascades a Fully Convolutional Network (FCN). The FCN is fed the features from both contracting block and expansive block, which has been shown to perform better in boundary detection [9]. The LF-UNet was trained on the RETOUCH dataset with the best state-of-art evaluation scores reported by MICCAI 2017 Satellite Event [6].

2 Methodologies

2.1 Traditional Method

Through visual inspection, the noise and intensity differences are evident between the two domains. Thus, without using machine learning, we inject Gaussian noise to visually match the two domains of data. The simple formula of Gaussian noise is:

$$P(x) = \frac{1}{\sigma\sqrt{2\pi}}e^{-(x-\mu)^2/2\sigma^2}$$

We determined which regions to inject Gaussian noise by utilizing a simple density detection technique. If a pixel's density was larger than a specified threshold, we set the intensity to 196 (from 0 to 255) and no noise was added. Furthermore, if the value was larger than 225 and the neighbouring intensity density was low, noise was not added to the adjacent pixels. After determining the regions to inject noise, we introduced Gaussian noise accordingly to generate our traditionally processed images. The logic of this method is detailed in Figure 2.

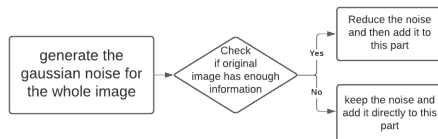


Figure 2: Traditional Mathematical Method

2.2 CycleGAN

CycleGAN was initially introduced in 2017, to learn bi-directional mapping functions between two different domains [10]. It emphasizes the concept of cycle consistency, where the reconstructed image obtained by a cyclic adaptation is expected to be identical to the original image. This regularization-purpose approach allows the adaptation for both domains, and it is widely used in many data-related applications.

2.2.1 Architecture

The architecture and main components of the network are shown below:

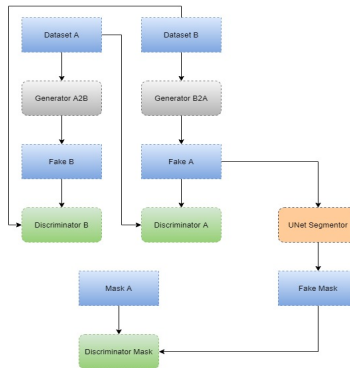


Figure 3: Flow diagram

As shown in Figure 3, CycleGAN consists of two main deep neural network blocks. Specifically, the generator and discriminator. The generator adapts the data from one domain to another, while the discriminator attempts to distinguish the generated images. DatasetA refers to RETOUCH B-scans, while datasetB refers to UKB B-scans. DatasetA was passed into the generatorA2B, then the generated images were passed to the discriminatorB along with the real datasetB. The same data-flow existed for datasetB, generatorB2A and discriminatorA, respectively. In addition to the basic CycleGAN, the segmentation data-flow was included. Since the LF-UNet was trained for segmenting B-scans from datasetA, the segmentation generated from both datasetA and generated image A was passed into the discriminator. The losses from both generators and discriminators were updated every epoch.

As shown in Figure 4 (a)(b), a detailed architecture for the core blocks is illustrated. The generator began with a 2x down-sampling operation for extracting deep features, then the feature maps were passed into 9 consecutive residual blocks, which is shown in Figure 4 (c). The residual block performs two sets of convolution and normalization layers with a ReLU activation function in between. The output was element-wise added with the input via a skip-connection to allow the network to learn simple functions like identity function

that may be difficult to capture using convolutional filters. After the series of residual blocks, the 2-x up-sampling operations were performed to reconstruct the feature maps in the other domain. The hyperbolic tangent activation (tanh) function was applied as the final rectifier. The discriminator was simpler than the generator and conducted 4-level feature reconstructions, followed by a 2D average pooling layer.

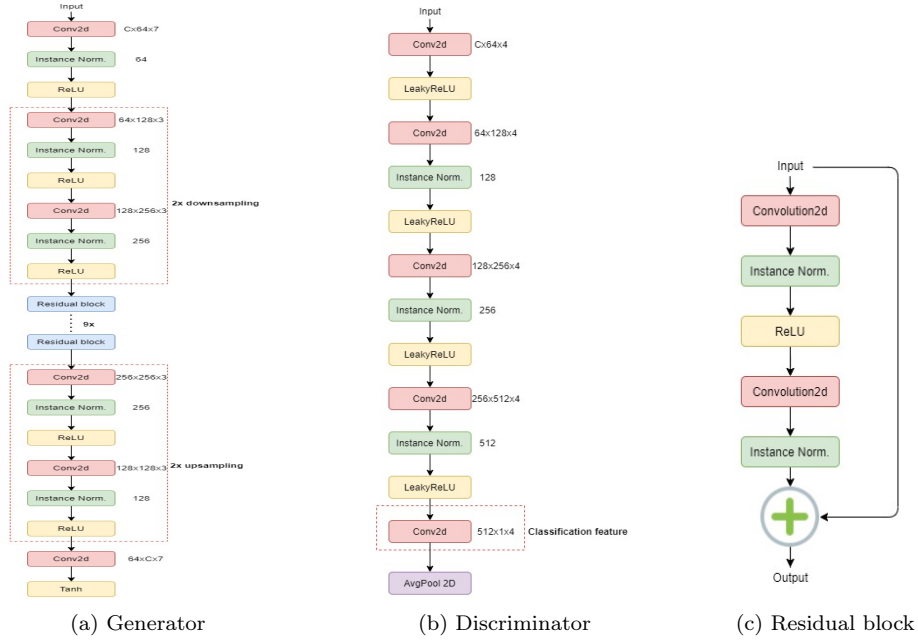


Figure 4: CycleGAN architecture and components

2.2.2 Loss functions

A Pytorch-implemented version was adopted as the baseline loss function for training the two OCT datasets [11]. The original paper mentioned two loss functions. Minimax loss, or adversarial loss, is designed to maximize the error of the discriminators. Given both generator G and discriminator D , and mapping function $G: X \rightarrow Y$, we have:

$$L_{GAN}(G, D_Y, X, Y) = E_{y \sim p_{data}(y)}[\log D_Y(y)] + E_{x \sim p_{data}(x)}[\log(1 - D_Y(G(x)))]$$

Also, for the reverse mapping function $F: Y \rightarrow X$, we have another one:

$$L_{GAN}(F, D_X, Y, X) = E_{x \sim p_{data}(x)}[\log D_X(x)] + E_{y \sim p_{data}(y)}[\log(1 - D_X(F(y)))]$$

The loss is minimized when the discriminator successfully distinguishes the input image. Therefore, a higher discriminator loss indicates a better performing

generator. Cycle consistency loss is defined based on the image reconstruction on both forward and backward direction:

$$L_{cyc}(G, F) = E_{x \sim p_{data}(x)}[\|F(G(x)) - x\|_1] + E_{y \sim p_{data}(y)}[\|G(F(y)) - y\|_1]$$

As the cycle loss decreases, the adapted image becomes more similar to the original image.

Two additional loss functions were added for better regularization. The identity loss was designed such that the generator performed no adaptation if the given input was from the output domain:

$$L_{id}(G, F) = E_{x \sim p_{data}(x)}[\|F(x) - x\|_1] + E_{y \sim p_{data}(y)}[\|G(y) - y\|_1]$$

The segmentation loss was designed to optimize such that the LF-UNet layer segmentation performance would be like that of the segmentation using the ground truth, UKB, data. The error was evaluated using both the dice loss and cross-entropy loss. Given the LF-UNet S and ground-truth segmentation M, we have:

$$L_{seg}(S, M, G) = E_{x \sim p_{data}(x)}[Dice(S(G(x)) - S(x))] + E_{y \sim p_{data}(y)}[CE(S(G(x)) - S(x))]$$

where the dice loss and cross-entropy loss is defined as:

$$Dice(A, B) = 1 - \frac{2|A \cap B|}{|A| + |B|} \text{ and } CE(p, q) = - \sum_{\forall x} p(x) \log(q(x))$$

The dice loss ensured that the overlap area is maximized, while the cross-entropy loss handled the over-segmentation issue by maximizing the pixel-wise probabilities.

2.2.3 Fine-tuning

The following fine-tuning process was inspired by multiple weighted loss approaches [12]. The author suggested three levels of regularization. First, the baseline network performs adaptation on pixel-wise aspect, where the feature maps may also guide the learning of the network. As shown in Figure 4 (b), the feature from the classification layer of the discriminator was extracted, which was added into the cycle consistency loss. Meanwhile, the feature weight γ was applied to focus the network on the pixel-wise information during early stages of training as the early features from discriminator would not have good quality, but the feature-level information would be weighted higher in later stages. Given the feature extractor from classification layer f_D and feature weight γ , we have:

$$L_{cyc}(G, F, D_X, X, \gamma) = E_{x \sim p_{data}(x)}[\gamma \|f_{D_X}(F(G(x))) - f_{D_X}(x)\|_1 + (1 - \gamma) \|F(G(x)) - x\|_1]$$

Second, a decaying weight λ was added to the modified cycle loss, so that the network is stabilizing quickly at early stages, and will not be constrained by cycle loss in later stages. The cycle loss then becomes:

$$L_{cyc}(G, F, D_X, X, \gamma) = E_{x \sim p_{data}(x)}[D_X(x)[\gamma \|f_{D_X}(F(G(x))) - f_{D_X}(x)\|_1 + (1 - \gamma) \|F(G(x)) - x\|_1]]$$

Last, the modified cycle loss from each direction was further weighted by the output of the corresponding discriminator. It helps with the cases when the generated fake images are unrealistic. The overall feature-weighted loss is:

$$L(G, F, D_X, D_Y, t) = L_{GAN}(G, D_Y, X, Y) + L_{GAN}(F, D_X, Y, X) + \lambda_t(L_{cyc}(G, F, D_X, X, \gamma_t) + L_{cyc}(F, G, D_Y, Y, \gamma_t) + L_{seg}(S, M, G))$$

3 Results

The two proposed methods, traditional Gaussian noise injection and CycleGAN, were both evaluated qualitatively, and quantitatively on three volumes of 128 b-scans.

3.1 Qualitative Evaluation

Visually, the segmentation produced from the methods proposed in the previous sections had varying results where the CycleGAN approach outperformed the traditional method, which outperformed the unprocessed FDA B-scans. This trend was consistent throughout all three volumes of the test set, as shown in Figure 5. In the left-most column, it can be seen that the intensity of the processed B-scans was overall increased as the method got more complex. The intensity was normalized prior to retina segmentation, thus, the absolute intensity value is not relevant. As shown in Figure 5, the segmentation of the unprocessed images is highly inaccurate and only segments the retina near the RPE. The traditional method of injecting Gaussian noise and intensity shifts performed extremely well in terms of retinal boundaries, but had many false negatives within the segmented retina. Domain adaptation through a CycleGAN resulted in the most visually appealing retina segmentation where the retinal boundaries are fairly consistent and there were rarely retinal pixels classified as background.

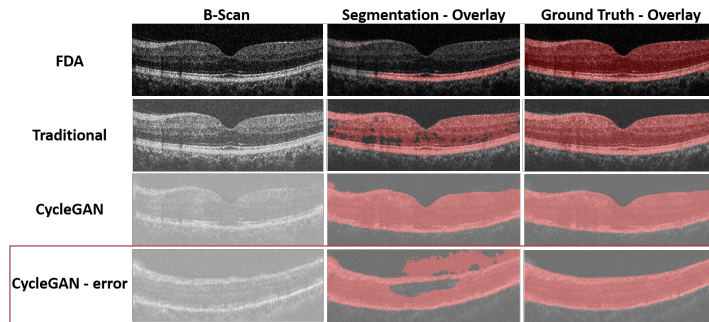


Figure 5: Retinal segmentation (red overlay) of the unprocessed (FDA), Gaussian noise (Traditional), machine learning (CycleGAN) approaches. An example of a poorly segmented B-scan is highlighted by the red box.

While this trend of visual performance was consistent throughout most of the test volumes, there were outliers where the CycleGAN domain adaptation resulted in poor inference, as shown in the highlighted row of Figure 5. While visual inspection suggested a subjective preference for CycleGAN over the traditional method, a quantitative analysis will allow an objective comparison.

3.2 Quantitative Evaluation

With reference to the Literature, the following performance metrics were calculated between the segmentation and ground truth for quantitative evaluation: accuracy [13][14], Dice Similarity Coefficient (DSC) [13][14], Jaccard Score (JS) [13], and area under the curve of the receiver operating characteristic (AUC) [13]. The UKB processing methods resulted in the segmentation performances from tools trained on the RETOUCH dataset, as shown in Table 1. Figure 6 graphically represents the segmentation performance of each method for all of the above evaluation metrics extensively used in the Literature.

Table 1: Domain adaptation performance through segmentation evaluation metrics. Formatted as follows: Mean (Standard Deviation).

	Baseline	Traditional	CycleGAN
Accuracy	0.869 (0.021)	0.969 (0.017)	0.978 (0.011)
JS	0.221 (0.108)	0.822 (0.096)	0.883 (0.055)
DSC	0.349 (0.014)	0.899 (0.062)	0.937 (0.032)
AUC	0.611 (0.055)	0.924 (0.051)	0.977 (0.015)

In the box plot, the light blue, purple, and red distributions represent the unprocessed FDA UKB, tradition Gaussian noise injection, and AI CycleGAN approaches, respectively. Statistical significance ($P < 0.05$) of the difference in means was calculated using two-tailed t-tests and highlighted by a red asterisk. Across all metrics, there was a statistically significant preference from the segmentation tools trained on the RETOUCH data for UKB adapted through CycleGAN over the traditional method, which in turn had a statistically significant preference over the unprocessed UKB data.

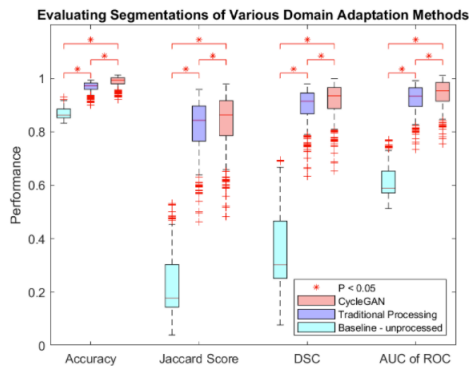


Figure 6: Segmentation evaluation metrics statistical analysis where statistically significant difference ($P < 0.05$) in means is highlighted by a red asterisk.

4 Conclusion

This study explored the performance of domain adaptation of drastically different data (UKB) to the domain used to train the OCT retinal layer segmentation tools. The retinal segmentation of the domain adaptation through a CycleGAN was compared to unprocessed, and traditional Gaussian noise injected retinal images. The segmentation on CycleGAN-adapted volumes was shown to be superior in accuracy, DSC, JS, and AUC. Future steps should be taken to explore the effect of CycleGAN on pathological eyes where the segmentation performance may be reduced. Regardless, the CycleGAN domain-adapted UKB data resulted in retinal inference with DSC of 0.937, which is comparable to the Literature which reports DSC ranging from 0.928 to 0.961 from different retinal layers [8]. In this domain adaptation experiment, from the perspective of adapting data to pretrained tools, the CycleGAN was significantly superior to a traditional-intensity-based approach.

References

- [1] American Diabetes Association "11. Microvascular Complications and Foot Care: Standards of Medical Care in Diabetes - 2020." *Diabetes Care* 43.Supplement 1 (2020): S135-S151.
- [2] Abràmoff, Michael D., et al. "Pivotal trial of an autonomous AI-based diagnostic system for detection of diabetic retinopathy in primary care offices." *NPJ digital medicine* 1.1 (2018): 1-8.
- [3] Kelly, Christopher J., et al. "Key challenges for delivering clinical impact with artificial intelligence." *BMC medicine* 17.1 (2019): 195.
- [4] Nagendran Myura, et al. "Artificial intelligence versus clinicians: systematic review of design, reporting standards, and claims of deep learning studies." *bmj* 368 (2020).
- [5] Abràmoff, Michael D., Danny Tobey, and Danton S. Char. "Lessons learnt about Autonomous AI: finding a safe, efficacious and ethical path through the development process." *American Journal of Ophthalmology* (2020).
- [6] Bogunović Hrvoje, et al. "RETOUCH: The retinal OCT fluid detection and segmentation benchmark and challenge." *IEEE transactions on medical imaging* 38.8 (2019): 1858-1874.
- [7] UK Biobank. Retrived from <https://www.ukbiobank.ac.uk/>
- [8] Donghuan Lu, Morgan Heisler, et al. *Cascaded Deep Neural Networks for Retinal Layer Segmentation of Optical Coherence Tomography with Fluid Presence* 2019
- [9] Olaf Ronneberger, Philipp Fischer, and Thomas Brox *U-Net: Convolutional Networks for Biomedical Image Segmentation* 2015
- [10] Jun-Yan, et al. *Unpaired Image-to-Image Translation using Cycle-Consistent Adversarial Networks.* *arXiv:1703.10593*
- [11] Aitor Ruano. Retrived from <https://github.com/aitorzip/PyTorch-CycleGAN>
- [12] Tongzhou W, et al. *CycleGAN with Better Cycles*
- [13] Jie W, et al. "Joint retina segmentation and classification for early glaucoma diagnosis." *Biomedical Optics Express* 10.5 (2019): 2639-2656.
- [14] Julian L, et al. "Microvasculature Segmentation and Intercapillary Area Quantification of the Deep Vascular Complex Using Transfer Learning." *Translational Vision Science & Technology* (2020): vol 9(2), pp. 38